

# Finite-volume effects in baryon number fluctuations around the QCD critical endpoint

Julian Bernhardt, Christian S. Fischer, Philipp Isserstedt

*Institut für Theoretische Physik, Justus-Liebig-Universität Gießen, 35392 Gießen, Germany*

*Helmholtz Forschungsakademie Hessen für FAIR (HFHF), GSI Helmholtzzentrum für Schwerionenforschung, Campus Gießen, 35392 Gießen, Germany*

---

## Abstract

We present results for the volume dependence of baryon number fluctuations in the vicinity of the (conjectured) critical endpoint of QCD. They are extracted from the nonperturbative quark propagator that is obtained as a solution to a set of truncated Dyson–Schwinger equations of  $(2 + 1)$ -flavor QCD in Landau gauge, which takes the backcoupling of quarks onto the Yang–Mills sector explicitly into account. This well-studied system predicts a critical endpoint at moderate temperatures and rather large chemical potential. We investigate this system at small and intermediate finite, three-dimensional, cubic volumes and study the resulting impact on baryon number fluctuations and ratios thereof up to fourth order around the critical endpoint. We find that the fluctuations are visibly affected by the finite volume, particularly for antiperiodic boundary conditions, whereas their ratios are practically invariant.

*Keywords:* QCD phase diagram, critical endpoint, baryon number fluctuations, finite-volume effects, Dyson–Schwinger equations

---

## 1. Introduction

Fluctuations of the conserved quantities baryon number, electromagnetic charge, and strangeness are important quantities in our quest to locate a potential critical endpoint (CEP) in the phase diagram of strong-interaction matter [1]. It is one of the main goals of the experimental programs at the Relativistic Heavy-Ion Collider at Brookhaven National Laboratory to find such an endpoint in a dedicated beam energy scan [2] that probes a large baryon-chemical-potential area of the phase diagram, which is not accessible at the Large Hadron Collider. The search for the CEP is also one of the main motivations for the future Compressed Baryonic Matter experiment [3] at the Facility of Antiproton and Ion Research in Darmstadt and the Nuclotron-based Ion Collider Facility at the Joint Institute for Nuclear Research in Dubna.

While at small chemical potentials an analytic crossover from the low-temperature hadronic phase to a high-temperature quark-gluon plasma phase has been firmly established, see Refs. [4–8] and references therein, the location where the crossover turns into a first-order phase transition—marked by a second-order CEP—is up to now not unambiguously determined. Elaborate calculations within the functional approach to QCD using sets of coupled Dyson–Schwinger or functional renormalization group (FRG) equations [9–14] place the endpoint into the region  $(\mu_B^{\text{CEP}}, T_{\text{CEP}}) = (495\text{--}654, 108\text{--}119)$  MeV, i.e., within a narrow temperature range with only moderate spread in chemical potential (see Fig. 1 below).

In experiments, signals for the CEP but also for the crossover and the first-order phase transition at large baryon chemical potential are expected to appear in ratios of event-by-event fluctuations, i.e., cumulants and related quantities. These may be particularly prominent in higher orders [15–19]. Ratios of cumulants have the advantage that the explicit volume dependence of the fluctuations drops out. However, as pointed out and investigated in Refs. [18, 20], implicit volume dependencies may remain. When comparing theoretical calculations with experimental results, these may have to be taken into account.

This is the topic of the present work. We study the explicit and implicit volume effects in baryon number fluctuations and ratios thereof in continuum QCD using the functional framework of Dyson–Schwinger equations (DSEs) at nonzero temperature and chemical potential. To this end, we use the truncation scheme of Refs. [10, 21] and investigate finite-volume effects for a range of cubic spatial volumes around the location of the CEP. We first detail our framework in Sec. 2. Then, we summarize the implementation of a finite spatial volume and the employed truncation scheme and provide the reader with the necessary information how fluctuations are determined in this framework. In Sec. 3, we discuss our results and conclude in Sec. 4.

## 2. Framework

### 2.1. Finite-volume generalities

Introducing a finite, uniform, three-dimensional cubic volume with edge length  $L$  amounts to the restriction of all appearing three-dimensional configuration-space integrals to the domain  $[0, L]^3 \subset \mathbb{R}^3$ . Imposing either periodic or antiperiodic boundary conditions (PBC or ABC, respectively) in the spatial directions,

---

*Email addresses:* julian.bernhardt@physik.uni-giessen.de (Julian Bernhardt), christian.fischer@theo.physik.uni-giessen.de (Christian S. Fischer), philipp.isserstedt@physik.uni-giessen.de (Philipp Isserstedt)

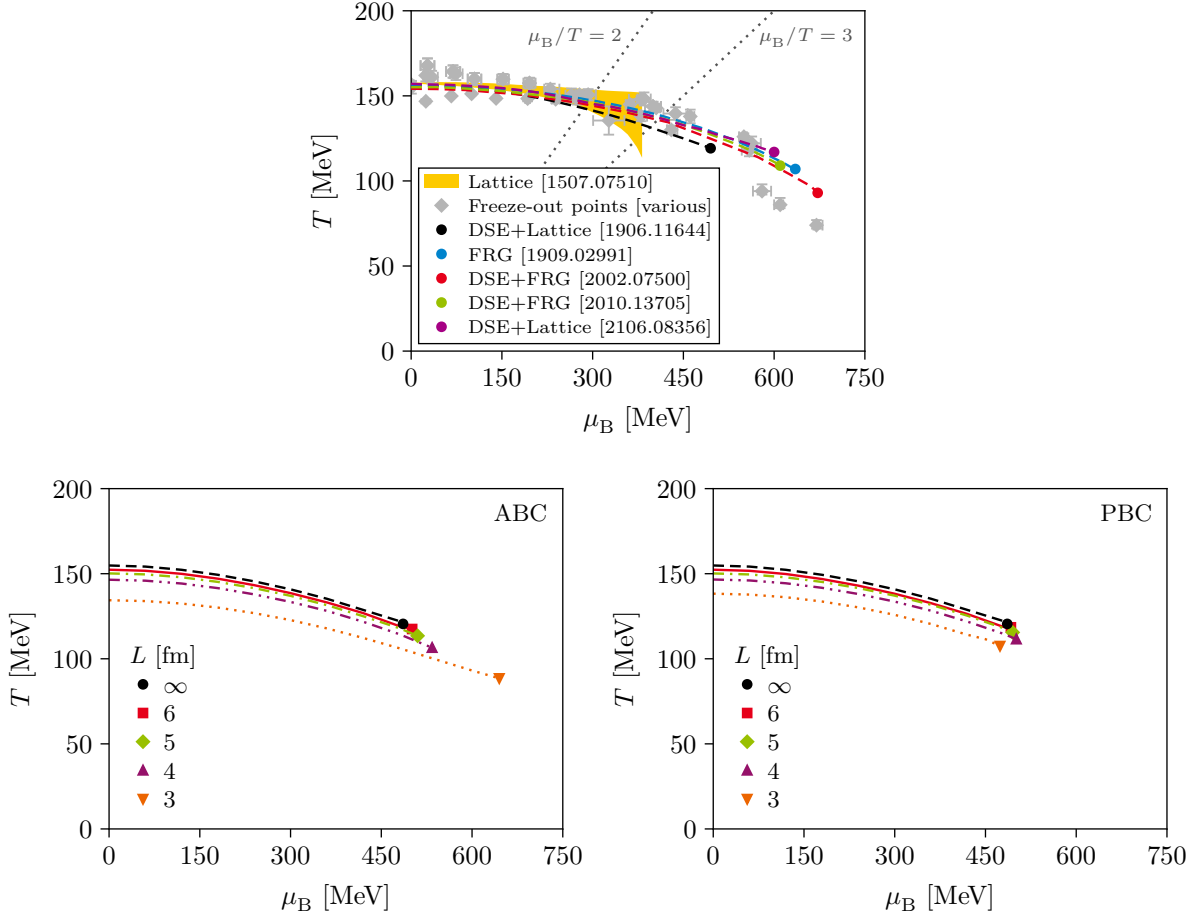


Figure 1: Upper diagram: various results for the analytic crossover and the CEP from state-of-the-art functional calculations [10–14] in comparison to an extrapolation from lattice QCD [22] and experimental freeze-out points [23–28]. Lower diagrams: volume dependence of the CEP of Ref. [10] as determined in Ref. [21] using antiperiodic (ABC) and periodic (PBC) spatial boundary conditions. We use a cubic volume  $V = L^3$ , where  $L$  denotes the edge length.

each momentum-space integral is therefore replaced by a sum over discrete spatial modes according to

$$\int \frac{d^3q}{(2\pi)^3} (\dots)(\mathbf{q}) \rightarrow \frac{1}{L^3} \sum_{\xi \in \mathbb{Z}^3} (\dots)(\mathbf{q}_\xi) \quad (1)$$

with  $\mathbf{q}_\xi = [\varpi_{\xi_1}, \varpi_{\xi_2}, \varpi_{\xi_3}]^\top$  and  $\xi \in \mathbb{Z}^3$ , where the spatial Matsubara modes are given by ( $i = 1, 2, 3$ )

$$\varpi_{\xi_i} = \frac{2\pi}{L} \times \begin{cases} \xi_i + 1/2 & \text{for ABC,} \\ \xi_i & \text{for PBC.} \end{cases} \quad (2)$$

When implementing a finite spatial volume in practical DSE calculations, it is

- (i) beneficial to rearrange the sum in Eq. (1) such that it resembles a spherical coordinate system [29];
- (ii) vital to remove finite-size artifacts, which are caused by the mismatch of the discrete momentum grid and the  $O(3)$ -symmetric continuum at large momenta;
- (iii) necessary to pay attention to the proper inclusion of the zero mode  $\mathbf{q}_{\xi=0} = \mathbf{0}$  that appears for PBC.

Since a detailed discussion of (i)–(iii) can be found in our previous work [21], we shall keep this section concise and refer the reader to that work for more details.

## 2.2. Dyson–Schwinger equations

Generally, the functional approach works with differential and/or integral equations, relating loops of nonperturbative correlation functions with each other. These can be formulated in configuration space or, much more common, in momentum space.

As in our previous work [21], we use DSEs to investigate QCD in a finite, three-dimensional cubic volume and at nonzero temperature  $T$  and quark chemical potential  $\mu_f$ , where  $f$  labels the flavor. The central quantity is the dressed quark propagator  $S_f$  that takes the form<sup>1</sup>

$$S_f^{-1}(\omega_n, \mathbf{p}_\zeta) = i\gamma_4(\omega_n + i\mu_f)C_f(\omega_n, \mathbf{p}_\zeta) + i\boldsymbol{\gamma} \cdot \mathbf{p}_\zeta A_f(\omega_n, \mathbf{p}_\zeta) + B_f(\omega_n, \mathbf{p}_\zeta) \quad (3)$$

<sup>1</sup>We work within the Matsubara (imaginary time) formalism, i.e., in Euclidean space-time with positive metric signature (++++). The gamma matrices are Hermitian and obey  $\{\gamma_\nu, \gamma_\sigma\} = 2\delta_{\nu\sigma}$ .



Figure 2: The DSE for the quark propagator. Large filled dots indicate dressed quantities; solid and curly lines represent quark and gluon propagators, respectively. There is a separate DSE for each flavor.

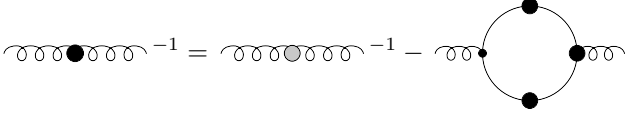


Figure 3: Truncated gluon DSE. The large gray dot denotes the quenched gluon propagator that is taken from the lattice while the quark loop is evaluated explicitly. The latter contains an implicit flavor sum.

with temporal Matsubara frequencies  $\omega_n = (2n + 1)\pi T$ ,  $n \in \mathbb{Z}$ , and  $\mathbf{p}_\zeta = [\varpi_{\zeta_1}, \varpi_{\zeta_2}, \varpi_{\zeta_3}]^\top$ ,  $\zeta \in \mathbb{Z}^3$ . The dressing functions  $A_f$ ,  $B_f$ , and  $C_f$  carry the nonperturbative information, which manifests in a nontrivial dependence on the Matsubara frequency and three-momentum.

The dressed quark propagator is the solution of its corresponding DSE that reads

$$S_f^{-1}(\omega_n, \mathbf{p}_\zeta) = Z_2 (i\gamma_4(\omega_n + i\mu_f) + i\boldsymbol{\gamma} \cdot \mathbf{p}_\zeta + Z_m m_f) - \Sigma_f(\omega_n, \mathbf{p}_\zeta), \quad (4)$$

where  $Z_2$ ,  $Z_m$ , and  $m_f$  denote the wave function renormalization constant, mass renormalization constant, and current quark mass, respectively. The former are determined in vacuum using a momentum-subtraction scheme. The self-energy is explicitly given by

$$\Sigma_f(\omega_n, \mathbf{p}_\zeta) = (ig)^2 \frac{4}{3} \frac{Z_2}{\tilde{Z}_3} \frac{T}{L^3} \sum_{k \in \mathbb{Z}} \sum_{\xi \in \mathbb{Z}^3} D_{\nu\rho}(\omega_k - \omega_n, \mathbf{q}_\xi - \mathbf{p}_\zeta) \times \gamma_\nu S_f(\omega_k, \mathbf{q}_\xi) \Gamma_\rho^f(\omega_k, \mathbf{q}_\xi, \omega_n, \mathbf{p}_\zeta) \quad (5)$$

with the strong coupling constant  $g$ , ghost renormalization constant  $\tilde{Z}_3$ , and dressed gluon propagator  $D_{\nu\rho}$ ; two factors of  $ig$  from the vertices appear explicitly such that  $\Gamma_\rho^f$  denotes the reduced dressed quark-gluon vertex. Color d.o.f. are already traced out resulting in the prefactor  $4/3$  for  $N_c = 3$  colors.

Equation (4) is shown diagrammatically in Fig. 2. In order to solve this self-consistent equation for the dressed quark propagator  $S_f$ , we need to specify two yet unknown quantities: the dressed gluon propagator and the dressed quark-gluon vertex, which both fulfill their own DSEs. The truncation used here has been studied extensively in the past (see, e.g., Refs. [10, 14, 21, 30, 31] for recent works and Ref. [32] for a review) and is characterized as follows.

First, in the full gluon DSE, we replace all pure Yang–Mills diagrams by fits to quenched, temperature-dependent lattice results [33, 34] while the quark loop is evaluated explicitly, thereby unquenching the gluon. The resulting equation is shown in Fig. 3. As a consequence, the quark and gluon DSEs are nontrivially coupled. This results in a temperature and (implicit) chemical-potential dependence of the gluon beyond modeling; moreover,

the gluon becomes sensitive to the chiral dynamics of the quarks. Though this approximation misses implicit quark-loop effects in the Yang–Mills self-energies, these are subleading in a skeleton expansion in comparison to the quark loop. The impact of this approximate yet efficient way to compute the unquenched gluon can be estimated in vacuum within the framework of Ref. [35] and is found to be below the five-percent level.

Second, for the dressed quark-gluon vertex, we use an ansatz that supplements the leading term of the Ball–Chiu vertex [36] with a phenomenological dressing function. The latter is constructed based on a Slavnov–Taylor identity for the full vertex together with the requirement of the correct logarithmic running of the propagators in the ultraviolet momentum region.

For the sake of brevity and since our setup is identical to the one used in previous works, we do not show explicit expressions and refer the reader to Refs. [10, 21, 32] and references therein for more details.<sup>2</sup>

The resulting set of truncated DSEs for the quark and gluon propagators is solved numerically. We use  $2 + 1$  quark flavors and work in the isospin-symmetric limit for the two light quarks, i.e.,  $m_u = m_d$  and  $\mu_u = \mu_d$ , and choose  $\mu_s = 0$ . Thus, the baryon chemical potential is given by  $\mu_B = 3\mu_u$ . The current quark masses are determined as follows (see Refs. [9, 10] for more details): (i) the up/down quark mass is chosen such that the high-temperature behavior of the regularized quark condensate matches lattice results [38]; (ii) the strange quark mass follows from the ratio  $m_s/m_u = 25.7$ , which is obtained from in-vacuum pion and kaon masses using the Bethe–Salpeter framework of Ref. [39].

### 2.3. Quark and baryon number fluctuations

In the following, we first briefly summarize some general aspects of fluctuations (see, e.g., Refs. [1, 40] for reviews) and then detail how we determine these from our solutions of the DSEs specified in the previous subsection.

In three-flavor QCD with quark chemical potentials  $\mu_u, \mu_d$ , and  $\mu_s$ , the quark number fluctuations are (dimensionless) derivatives of QCD’s thermodynamic potential  $\Omega$  with respect to these chemical potentials, viz.

$$\chi_{ijk}^{\text{uds}} = -\frac{1}{T^{4-(i+j+k)}} \frac{\partial^{i+j+k} \Omega}{\partial \mu_u^i \partial \mu_d^j \partial \mu_s^k} \quad (6)$$

with  $\Omega = -T \log(\mathcal{Z})/V$  and  $i, j, k \in \mathbb{N}$ , where  $\mathcal{Z}$  denotes the grand-canonical partition function of QCD and  $V$  the volume of the system. The quark chemical potentials are related to the ones for baryon number (B), electric charge (Q), and strangeness (S) via  $\mu_u = \mu_B/3 + 2\mu_Q/3$ ,  $\mu_d = \mu_B/3 - \mu_Q/3$ , and  $\mu_s = \mu_B/3 - \mu_Q/3 - \mu_S$ . With these relations, the corresponding fluctuations  $\chi_{ijk}^{\text{BQS}}$  can be expressed as linear combinations of quark number fluctuations. For example,

$$\chi_2^{\text{B}} = \frac{1}{9} [\chi_2^{\text{u}} + \chi_2^{\text{d}} + \chi_2^{\text{s}} + 2(\chi_{11}^{\text{ud}} + \chi_{11}^{\text{us}} + \chi_{11}^{\text{ds}})]. \quad (7)$$

<sup>2</sup>The fits to the quenched lattice gluon propagator can be found in the earlier work [37], and the quark-gluon vertex ansatz is discussed in detail in Ref. [9].

Generally, fluctuations of conserved charges are sensitive to phase transitions and thus expected to be prime candidates to provide signatures of the (conjectured) CEP in experiments. Ratios are particularly interesting because they are equal to ratios of cumulants of the corresponding probability distributions that can be extracted from heavy-ion collisions by means of event-by-event analyses; see Refs. [1, 2, 40, 41] and references therein for more details. Prominent ratios are the ones involving the skewness and kurtosis, namely

$$\frac{\chi_3^B}{\chi_2^B} = S_B \sigma_B, \quad \frac{\chi_4^B}{\chi_2^B} = \kappa_B \sigma_B^2, \quad (8)$$

where  $\sigma_B^2$ ,  $S_B$ , and  $\kappa_B$  denote the variance, skewness, and kurtosis of the net-baryon distribution, respectively. Analogous expressions hold for charge and strangeness.

In this work, we consider  $\chi_2^B$  and the skewness and kurtosis ratios, which are determined via the quark number fluctuations [see Eq. (7)]. As in our previous work [10], we compute the latter from the quark number densities  $n_f = -\partial\Omega/\partial\mu_f$ ; for instance,

$$\chi_2^u = \frac{1}{T^2} \frac{\partial n_u}{\partial \mu_u}. \quad (9)$$

In infinite volume, the regularized quark number density for a flavor  $f$  is obtained from the dressed quark propagator via [10]

$$n_f^{\text{reg}} = -N_c Z_2 K_f, \quad (10)$$

where

$$\begin{aligned} K_f &= T \sum_{k \in \mathbb{Z}} \int \frac{d^3 q}{(2\pi)^3} \text{Tr}[\gamma_4 S_f(\omega_k, \mathbf{q})] \\ &\quad - \int_{-\infty}^{\infty} \frac{dq_4}{2\pi} \int \frac{d^3 q}{(2\pi)^3} \text{Tr}[\gamma_4 S_f(q_4, \mathbf{q})] \\ &\equiv K_f^{\text{sum}} - K_f^{\text{int}}. \end{aligned} \quad (11)$$

The term  $K_f^{\text{sum}}$  contains the temporal Matsubara frequencies and is the one expected to yield the quark number density. However, it is divergent and needs to be regularized if—as in our approach—evaluated numerically where only a finite number of Matsubara frequencies is available. To this end, we subtract the term  $K_f^{\text{int}}$  that does not depend explicitly on temperature or chemical potential and is therefore known as a “vacuum contribution” [42]. This subtraction scheme is based on the Euclidean version of the contour-integration technique for Matsubara sums; see, e.g., Refs. [10, 43, 44] for more details.

In a finite volume, the expression for  $K_f$  turns into

$$\begin{aligned} K_f &= \frac{T}{L^3} \sum_{k \in \mathbb{Z}} \sum_{\xi \in \mathbb{Z}^3} \text{Tr}[\gamma_4 S_f(\omega_k, \mathbf{q}_\xi)] \\ &\quad - \int_{-\infty}^{\infty} \frac{dq_4}{2\pi} \int_{\text{ABC/PBC}} \frac{d^3 q}{(2\pi)^3} \text{Tr}[\gamma_4 S_f(q_4, \mathbf{q})], \end{aligned} \quad (12)$$

where we replaced the infinite-volume integral by the finite-volume sum with respect to spatial Matsubara sums in the first term  $K_f^{\text{sum}}$  but not in the subtraction term  $K_f^{\text{int}}$ . It turns

out that this procedure is necessary to avoid artifacts in the resulting densities related to the high-momentum behavior of the subtraction term. The subscript ABC/PBC of the integral indicates that we treat the radial integral differently for different boundary conditions: whereas there is no momentum gap for PBC and the integral consequently starts at zero, for ABC we have  $\mathbf{q}_{\xi=0}^{\text{ABC}} \neq \mathbf{0}$  and therefore set the lower integration limit to the value of the smallest possible momentum magnitude.

Before presenting our results, we would also like to briefly comment on numerical stability. First, due to the necessary subtraction, the quark number density itself is numerically rather sensitive already in the infinite-volume setup and, as it turns out, even more so in finite-volume calculations. Second, its derivatives, the fluctuations, are at present only accessible by means of finite-difference formulae. This leads to a limited accuracy with numerical uncertainties of the order of ten percent.

### 3. Results and discussion

Our starting point is the infinite-volume result for the location of the CEP from Ref. [10], which is displayed in the upper diagram of Fig. 1 together with recent results from other functional approaches [11–14] and an extrapolation obtained from lattice QCD [22]. As already discussed in the introduction, all results from these state-of-the-art functional calculations cluster in the region  $(\mu_B^{\text{CEP}}, T_{\text{CEP}}) = (495\text{--}654, 108\text{--}119)$  MeV. The size of this region can be viewed as a measure of the lower bound for the remaining systematic error of the functional approach because the employed truncations differ in many technical details but are roughly on a similar level regarding the overall treatment of the tower of FRG equations and DSEs.

In the following, we discuss finite-volume baryon number fluctuations and their ratios around the CEP and compare them to their infinite-volume limit, which is explicitly calculated using the framework of Ref. [10] (black dot in Fig. 1). We study cubes with edge lengths of  $L = 2.5, 3, 4, 5, 6,$  and  $8$  fm for both ABC and PBC.

We recall that the location of the CEP in the phase diagram is volume dependent—the corresponding calculations have been carried out in Ref. [21] and are shown again in the lower diagrams of Fig. 1. Sizable effects only occur for volumes  $V \lesssim (5 \text{ fm})^3$  and are much larger for ABC than for PBC. For the sake of comparability, in the following we always show results obtained around the respective critical chemical potential for each system size. Additionally, we also normalize all temperatures to the corresponding critical temperatures. Since fluctuations around the CEP vary rapidly with temperature, a dense numerical grid is necessary to avoid misalignments. We accomplish for that by using steps of one MeV in temperature.

#### 3.1. Baryon number fluctuations

We begin our discussion with the results for the baryon number fluctuations. In Fig. 4, we exemplarily show the second-order baryon number fluctuation  $\chi_2^B$  for both ABC (left) and PBC (right) at finite volume as well as the infinite-volume result in black for comparison.

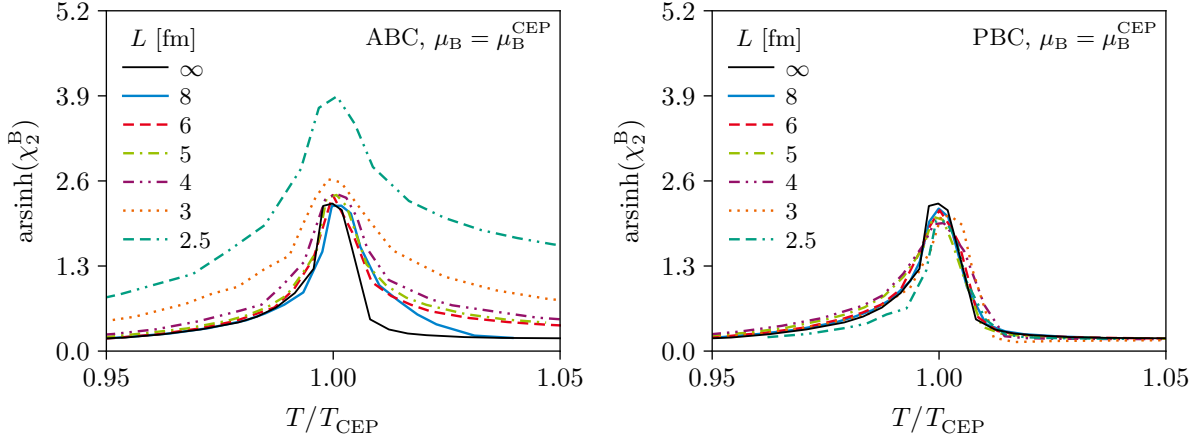


Figure 4: Volume dependence of the second-order baryon number fluctuation for ABC (left) and PBC (right) in the vicinity of the CEP. We plot the fluctuations at the volume-dependent chemical potential of the CEP,  $\mu_B = \mu_B^{\text{CEP}}(L)$ , as functions of the reduced temperature  $T/T_{\text{CEP}}$ , where  $T_{\text{CEP}} = T_{\text{CEP}}(L)$  is the volume-dependent temperature of the CEP. For better visibility, we display the inverse hyperbolic sine (arsinh) of the fluctuations, which resembles a logarithmic plot in both positive and negative direction.

Starting with the ABC results, we find clearly visible volume effects. That is, we see a monotonous increase of  $\chi_2^B$  with decreasing system size across the whole temperature range. The  $L = 2.5$  fm line especially stands out with the arsinh of its peak value nearly being doubled as compared to the infinite-volume result. For  $T < T_{\text{CEP}}$ , we find a consistent infinite-volume limit, i.e., the results for  $L \gtrsim 5$  fm are very similar to one another, while the  $L = 8$  fm line coincides with the infinite-volume one. For  $T > T_{\text{CEP}}$ , however, we see noticeable deviations between the finite- and infinite-volume results. We have not succeeded to track down these deviations unambiguously, but we believe they originate from the finite-volume adjusted subtraction procedure of the density outlined in Sec. 2.3 either as remnants or as an overcompensation of the initial problem.

In contrast, the fluctuations using PBC shown in the right diagram of Fig. 4 are much less dependent on the volume of the system than the fluctuations with ABC. This resembles similar differences between PBC and ABC effects on the location of the CEP discussed above. In fact, the volume dependence of the fluctuations with PBC are within our margin of error. Nonetheless, for  $T < T_{\text{CEP}}$ , one can observe a monotonous increase of  $\chi_2^B$  with decreasing system size down to  $L = 4$  fm. For smaller box sizes, the values start decreasing again. This behavior is similar to the nonmonotonous volume dependence of the location of the CEP around  $L = 3$  fm that has been already noticed in Ref. [21]. It may be linked to the onset of the so-called epsilon regime at very small volumes [45].

In addition, the infinite-volume limit of the PBC fluctuations is much more consistent for  $T > T_{\text{CEP}}$  as compared to ABC. That is, there are no substantial deviations between the  $L = 8$  fm and the  $L \rightarrow \infty$  lines. As a consequence, one might conjecture that the numerical problems of ABC for  $T > T_{\text{CEP}}$  are connected to infrared momentum modes because ABC introduce an effective infrared cutoff,  $q_{\xi=0}^{\text{ABC}} \neq \mathbf{0}$ , while PBC do not,  $q_{\xi=0}^{\text{PBC}} = \mathbf{0}$ .

We also extracted the peak heights of the ABC and PBC results for  $\chi_2^B$  as a function of volume and analyzed their behavior in terms of power laws. Whereas the PBC results are virtually

independent of volume, i.e., roughly proportional to  $V^0$ , there is no clear power-law behavior visible for the ABC results if all volumes are considered. This may or may not be connected to the numerical error discussed at the end of Sec. 2.3 and needs to be revisited in the future in a more refined framework. Interestingly, as we will confirm in the next subsection, the volume dependence is similar for the higher-order fluctuations, too.

### 3.2. Ratios of baryon number fluctuations

Next, we turn to ratios of baryon number fluctuation. To this end, we display (the inverse hyperbolic sine of) both the skewness and kurtosis ratios for ABC and PBC in Fig. 5. For comparison, the infinite-volume result is again shown as a black line. In general, one can observe that both ratios for both boundary conditions and all system sizes qualitatively coincide very well for  $T \leq T_{\text{CEP}}$ . Additionally, they are also compatible with the respective infinite-volume results.

For ABC, however, we find again slight inconsistencies between the finite- and infinite-volume data for  $T > T_{\text{CEP}}$ . Neglecting the obvious outlier at  $L = 8$  fm, the lines of the larger volumes deviate qualitatively from the  $L \rightarrow \infty$  one, especially for larger temperatures. This deviation is more pronounced for the skewness ratio. Contrary to this, the PBC results exhibit once more no such behavior, and we observe a consistent infinite-volume limit also for  $T > T_{\text{CEP}}$ . In fact, the  $L = 8$  fm and the infinite-volume curves are almost indistinguishable. This seems to corroborate our assumption that the infrared cutoff of ABC leads to some numerical problems for  $T > T_{\text{CEP}}$ .

In addition to that, there are two notable outliers: the curves for ABC at  $L = 8$  fm and PBC at  $L = 3$  fm. Due to the randomness in their occurrence, they are most likely of purely numerical origin. We remark that the deviation from the rest of the curves in both cases occurs again for  $T > T_{\text{CEP}}$ , which makes a connection to the subtraction procedure plausible. This also implies that PBC are not completely immune to these numerical problems.

Overall, we find the remarkable result that all individual volume dependencies of the fluctuations cancel once ratios are

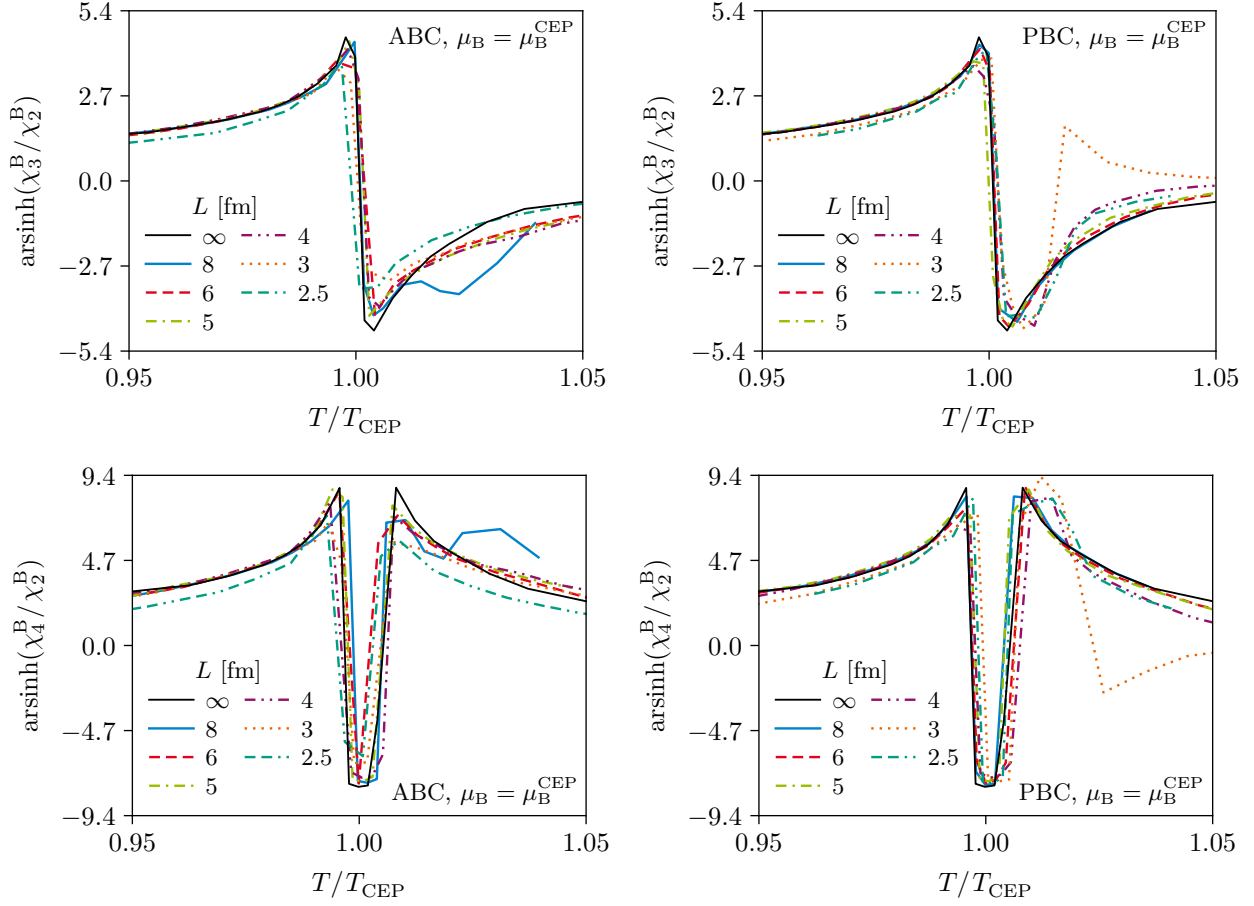


Figure 5: Volume dependence of the skewness (top) and kurtosis (bottom) ratios for ABC (left) and PBC (right) in the vicinity of the CEP. The way we plot the fluctuations is identical to Fig. 4.

studied. This not only true for large volumes but also for our smallest system sizes of  $L = 5, 4, 3,$  and  $2.5$  fm. This is somewhat in contrast to the results of Ref. [20], where significant volume effects in the kurtosis ratio have been found for volumes  $V \lesssim (5 \text{ fm})^3$  within an FRG treatment of the quark-meson model. Since the two approaches are rather different, e.g., our approach treats the gluonic sector explicitly but neglects a class of mesonic fluctuations, and vice versa in their approach, it may be interesting to provide a systematic comparison in the future.

#### 4. Summary and conclusions

In this work, we determined the volume dependence of the skewness and kurtosis ratios of baryon number fluctuations within a well-established functional approach to QCD. For a wide range of cubic spatial volumes with edge lengths between  $L = 2.5$  fm and  $L = 8$  fm and two different boundary conditions (ABC and PBC), we observe almost no volume dependence of these ratios. This is a highly nontrivial result because the individual results for the different fluctuations, both for ABC and for PBC, reveal a pattern that is at odds with the general expectation of linear dependence on volume: whereas the PBC results for  $\chi_2^B$  do not change with volume, the ones for ABC are even inversely proportional to  $V = L^3$ . Nevertheless, all these

dependencies cancel in the ratios, which are important when comparing with experimental results from heavy-ion collisions. We consider this a highly encouraging and relevant result.

#### Acknowledgments

We thank Jana N. Guenther for enlightening discussions. This work has been supported by the Helmholtz Graduate School for Hadron and Ion Research (HGS-HIRE) for FAIR, the GSI Helmholtzzentrum für Schwerionenforschung, and the Bundesministerium für Bildung und Forschung (BMBF) under Contract No. 05P18RGFCA. Feynman diagrams were drawn with JAXODRAW [46].

#### References

- [1] X. Luo, N. Xu, Search for the QCD critical point with fluctuations of conserved quantities in relativistic heavy-ion collisions at RHIC: an overview, Nucl. Sci. Tech. 28 (2017) 112. [arXiv:1701.02105](https://arxiv.org/abs/1701.02105), [doi:10.1007/s41365-017-0257-0](https://doi.org/10.1007/s41365-017-0257-0).
- [2] A. Bzdak, et al., Mapping the phases of quantum chromodynamics with beam energy scan, Phys. Rep. 853 (2020) 1. [arXiv:1906.00936](https://arxiv.org/abs/1906.00936), [doi:10.1016/j.physrep.2020.01.005](https://doi.org/10.1016/j.physrep.2020.01.005).
- [3] B. Friman, et al. (Eds.), The CBM Physics Book: Compressed Baryonic Matter in Laboratory Experiments, no. 814 in Lecture Notes in Physics, Springer, 2011. [doi:10.1007/978-3-642-13293-3](https://doi.org/10.1007/978-3-642-13293-3).

- [4] H. T. Ding, et al., Chiral Phase Transition Temperature in (2 + 1)-Flavor QCD, *Phys. Rev. Lett.* 123 (2019) 062002. [arXiv:1903.04801](#), [doi:10.1103/PhysRevLett.123.062002](#).
- [5] A. Bazavov, et al., Skewness, kurtosis, and the fifth and sixth order cumulants of net baryon-number distributions from lattice QCD confront high-statistics STAR data, *Phys. Rev. D* 101 (2020) 074502. [arXiv:2001.08530](#), [doi:10.1103/PhysRevD.101.074502](#).
- [6] S. Borsányi, et al., QCD Crossover at Finite Chemical Potential from Lattice Simulations, *Phys. Rev. Lett.* 125 (2020) 052001. [arXiv:2002.02821](#), [doi:10.1103/PhysRevLett.125.052001](#).
- [7] J. N. Guenther, Overview of the QCD phase diagram: Recent progress from the lattice, *Eur. Phys. J. A* 57 (2021) 136. [arXiv:2010.15503](#), [doi:10.1140/epja/s10050-021-00354-6](#).
- [8] S. Borsányi, et al., Lattice QCD Equation of State at Finite Chemical Potential from an Alternative Expansion Scheme, *Phys. Rev. Lett.* 126 (2021) 232001. [arXiv:2102.06660](#), [doi:10.1103/PhysRevLett.126.232001](#).
- [9] C. S. Fischer, J. Luecker, C. A. Welzbacher, Phase structure of three and four flavor QCD, *Phys. Rev. D* 90 (2014) 034022. [arXiv:1405.4762](#), [doi:10.1103/PhysRevD.90.034022](#).
- [10] P. Isserstedt, M. Buballa, C. S. Fischer, P. J. Gunkel, Baryon number fluctuations in the QCD phase diagram from Dyson–Schwinger equations, *Phys. Rev. D* 100 (2019) 074011. [arXiv:1906.11644](#), [doi:10.1103/PhysRevD.100.074011](#).
- [11] W.-j. Fu, J. M. Pawłowski, F. Rennecke, QCD phase structure at finite temperature and density, *Phys. Rev. D* 101 (2020) 054032. [arXiv:1909.02991](#), [doi:10.1103/PhysRevD.101.054032](#).
- [12] F. Gao, J. M. Pawłowski, QCD phase structure from functional methods, *Phys. Rev. D* 102 (2020) 034027. [arXiv:2002.07500](#), [doi:10.1103/PhysRevD.102.034027](#).
- [13] F. Gao, J. M. Pawłowski, Chiral phase structure and critical end point in QCD, *Phys. Lett. B* 820 (2021) 136584. [arXiv:2010.13705](#), [doi:10.1016/j.physletb.2021.136584](#).
- [14] P. J. Gunkel, C. S. Fischer, Locating the critical endpoint of QCD: Mesonic backcoupling effects, *Phys. Rev. D* 104 (2021) 054022. [arXiv:2106.08356](#), [doi:10.1103/PhysRevD.104.054022](#).
- [15] M. A. Stephanov, K. Rajagopal, E. V. Shuryak, Signatures of the Tricritical Point in QCD, *Phys. Rev. Lett.* 81 (1998) 4816. [arXiv:hep-ph/9806219](#), [doi:10.1103/PhysRevLett.81.4816](#).
- [16] M. A. Stephanov, K. Rajagopal, E. V. Shuryak, Event-by-event fluctuations in heavy ion collisions and the QCD critical point, *Phys. Rev. D* 60 (1999) 114028. [arXiv:hep-ph/9903292](#), [doi:10.1103/PhysRevD.60.114028](#).
- [17] B. Friman, F. Karsch, K. Redlich, V. Skokov, Fluctuations as probe of the QCD phase transition and freeze-out in heavy ion collisions at LHC and RHIC, *Eur. Phys. J. C* 71 (2011) 1694. [arXiv:1103.3511](#), [doi:10.1140/epjc/s10052-011-1694-2](#).
- [18] V. Skokov, B. Friman, K. Redlich, Volume fluctuations and higher-order cumulants of the net baryon number, *Phys. Rev. C* 88 (2013) 034911. [arXiv:1205.4756](#), [doi:10.1103/PhysRevC.88.034911](#).
- [19] A. Bzdak, V. Koch, N. Strodthoff, Cumulants and correlation functions versus the QCD phase diagram, *Phys. Rev. C* 95 (2017) 054906. [arXiv:1607.07375](#), [doi:10.1103/PhysRevC.95.054906](#).
- [20] G. A. Almási, R. D. Pisarski, V. Skokov, Volume dependence of baryon number cumulants and their ratios, *Phys. Rev. D* 95 (2017) 056015. [arXiv:1612.04416](#), [doi:10.1103/PhysRevD.95.056015](#).
- [21] J. Bernhardt, C. S. Fischer, P. Isserstedt, B.-J. Schaefer, Critical endpoint of QCD in a finite volume, *Phys. Rev. D* 104 (2021) 074035. [arXiv:2107.05504](#), [doi:10.1103/PhysRevD.104.074035](#).
- [22] R. Bellwied, S. Borsányi, Z. Fodor, J. Günther, S. D. Katz, C. Ratti, K. K. Szabó, The QCD phase diagram from analytic continuation, *Phys. Lett. B* 751 (2015) 559. [arXiv:1507.07510](#), [doi:10.1016/j.physletb.2015.11.011](#).
- [23] P. Alba, et al., Freeze-out conditions from net-proton and net-charge fluctuations at RHIC, *Phys. Lett. B* 738 (2014) 305. [arXiv:1403.4903](#), [doi:10.1016/j.physletb.2014.09.052](#).
- [24] V. Vovchenko, V. V. Begun, M. I. Gorenstein, Hadron multiplicities and chemical freeze-out conditions in proton-proton and nucleus-nucleus collisions, *Phys. Rev. C* 93 (2016) 064906. [arXiv:1512.08025](#), [doi:10.1103/PhysRevC.93.064906](#).
- [25] F. Becattini, J. Steinheimer, R. Stock, M. Bleicher, Hadronization conditions in relativistic nuclear collisions and the QCD pseudo-critical line, *Phys. Lett. B* 764 (2017) 241. [arXiv:1605.09694](#), [doi:10.1016/j.physletb.2016.11.033](#).
- [26] A. Andronic, P. Braun-Munzinger, K. Redlich, J. Stachel, Hadron yields, the chemical freeze-out and the QCD phase diagram, *J. Phys. Conf. Ser.* 779 (2017) 012012. [arXiv:1611.01347](#), [doi:10.1088/1742-6596/779/1/012012](#).
- [27] L. Adamczyk, et al., Bulk properties of the medium produced in relativistic heavy-ion collisions from the beam energy scan program, *Phys. Rev. C* 96 (2017) 044904. [arXiv:1701.07065](#), [doi:10.1103/PhysRevC.96.044904](#).
- [28] A. Andronic, P. Braun-Munzinger, K. Redlich, J. Stachel, Decoding the phase structure of QCD via particle production at high energy, *Nature* 561 (2018) 321. [arXiv:1710.09425](#), [doi:10.1038/s41586-018-0491-6](#).
- [29] C. S. Fischer, R. Alkofer, H. Reinhardt, The elusiveness of infrared critical exponents in Landau gauge Yang–Mills theories, *Phys. Rev. D* 65 (2002) 094008. [arXiv:hep-ph/0202195](#), [doi:10.1103/PhysRevD.65.094008](#).
- [30] P. J. Gunkel, C. S. Fischer, P. Isserstedt, Quarks and light (pseudo-)scalar mesons at finite chemical potential, *Eur. Phys. J. A* 55 (2019) 169. [arXiv:1907.08110](#), [doi:10.1140/epja/i2019-12868-1](#).
- [31] P. Isserstedt, C. S. Fischer, T. Steinert, Thermodynamics from the quark condensate, *Phys. Rev. D* 103 (2021) 054012. [arXiv:2012.04991](#), [doi:10.1103/PhysRevD.103.054012](#).
- [32] C. S. Fischer, QCD at finite temperature and chemical potential from Dyson–Schwinger equations, *Prog. Part. Nucl. Phys.* 105 (2019) 1. [arXiv:1810.12938](#), [doi:10.1016/j.pnpnp.2019.01.002](#).
- [33] C. S. Fischer, A. Maas, J. A. Mueller, Chiral and deconfinement transition from correlation functions: SU(2) vs. SU(3), *Eur. Phys. J. C* 68 (2010) 165. [arXiv:1003.1960](#), [doi:10.1140/epjc/s10052-010-1343-1](#).
- [34] A. Maas, J. M. Pawłowski, L. von Smekal, D. Spielmann, The gluon propagator close to criticality, *Phys. Rev. D* 85 (2012) 034037. [arXiv:1110.6340](#), [doi:10.1103/PhysRevD.85.034037](#).
- [35] C. S. Fischer, R. Alkofer, Nonperturbative propagators, running coupling, and the dynamical quark mass of Landau gauge QCD, *Phys. Rev. D* 67 (2003) 094020. [arXiv:hep-ph/0301094](#), [doi:10.1103/PhysRevD.67.094020](#).
- [36] J. S. Ball, T.-W. Chiu, Analytic properties of the vertex function in gauge theories. I, *Phys. Rev. D* 22 (1980) 2542. [doi:10.1103/PhysRevD.22.2542](#).
- [37] G. Eichmann, C. S. Fischer, C. A. Welzbacher, Baryon effects on the location of QCD’s critical end point, *Phys. Rev. D* 93 (2016) 034013. [arXiv:1509.02082](#), [doi:10.1103/PhysRevD.93.034013](#).
- [38] S. Borsányi, et al., Is there still any  $T_c$  mystery in lattice QCD? Results with physical masses in the continuum limit III, *J. High Energy Phys.* 09 (2010) 73. [arXiv:1005.3508](#), [doi:10.1007/JHEP09\(2010\)073](#).
- [39] W. Heupel, T. Goecke, C. S. Fischer, Beyond rainbow-ladder in bound state equations, *Eur. Phys. J. A* 50 (2014) 85. [arXiv:1402.5042](#), [doi:10.1140/epja/i2014-14085-x](#).
- [40] M. Asakawa, M. Kitazawa, Fluctuations of conserved charges in relativistic heavy ion collisions: An introduction, *Prog. Part. Nucl. Phys.* 90 (2016) 299. [arXiv:1512.05038](#), [doi:10.1016/j.pnpnp.2016.04.002](#).
- [41] V. Koch, Hadronic Fluctuations and Correlations, Springer, 2010. [arXiv:0810.2520](#), [doi:10.1007/978-3-642-01539-7\\_20](#).
- [42] J. I. Kapusta, C. Gale, Finite-Temperature Field Theory: Principles and Applications, 2nd Edition, Cambridge University Press, 2006. [doi:10.1017/CBO9780511535130](#).
- [43] F. Gao, Y.-x. Liu, Interface effect in QCD phase transitions via Dyson–Schwinger equation approach, *Phys. Rev. D* 94 (2016) 094030. [arXiv:1609.08038](#), [doi:10.1103/PhysRevD.94.094030](#).
- [44] P. Isserstedt, Thermodynamics of strong-interaction matter: On the phase structure and thermodynamics of quantum chromodynamics with Dyson–Schwinger equations, Ph.D. thesis, Giessen University, Germany (2021). [doi:10.22029/jlupub-310](#).
- [45] H. Leutwyler, A. V. Smilga, Spectrum of Dirac operator and role of winding number in QCD, *Phys. Rev. D* 46 (1992) 5607. [doi:10.1103/PhysRevD.46.5607](#).
- [46] D. Binosi, J. Collins, C. Kaufhold, L. Theussl, JaxoDraw: A graphical user interface for drawing Feynman diagrams. Version 2.0 release notes, *Comput. Phys. Commun.* 180 (2009) 1709. [arXiv:0811.4113](#), [doi:10.1016/j.cpc.2009.02.020](#).